



1 **Precise dating of deglacial Laptev Sea sediments via ^{14}C and**
2 **authigenic $^{10}\text{Be}/^9\text{Be}$ – assessing local ^{14}C reservoir ages**

3
4 Arnaud Nicolas^{1,2}, Gesine Mollenhauer^{1,2,3}, Johannes Lachner⁴, Konstanze Stübner⁴, Maylin
5 Malter¹, Jutta Wollenburg¹, Hendrik Grotheer^{1,3}, Florian Adolphi^{1,2}

6
7 ¹Alfred Wegener Institute, Bremerhaven, Germany

8 ²Department of Geosciences, University of Bremen, Bremen, Germany

9 ³MARUM-Center for Marine Environmental Sciences, University of Bremen, Bremen, Germany

10 ⁴Helmholz-Zentrum Dresden-Rossendorf, Dresden, Germany

11

12 Correspondence: Arnaud Nicolas (arnaud.nicolas@awi.de) and Florian Adolphi (florian.adolphi@awi.de)

13

14 **Abstract**

15

16 Establishing accurate chronological frameworks is imperative for reliably identifying lead-lag dynamics within
17 the climate system and enabling meaningful inter-comparisons across diverse paleoclimate proxy records over
18 long time periods. Robust age models provide a solid temporal foundation for establishing correlations between
19 paleoclimate records. One of the primary challenges in constructing reliable radiocarbon-based chronologies in
20 the marine environment is to determine the regional marine radiocarbon reservoir age correction. Calculations of
21 the local marine reservoir effect (ΔR) can be acquired using ^{14}C -independent dating methods, such as
22 synchronization with other well-dated archives. The cosmogenic radionuclide ^{10}Be offers such a synchronization
23 tool. Its atmospheric production rate is controlled by the global changes in the cosmic ray influx, caused by
24 variations in solar activity and geomagnetic field strength. The resulting fluctuations in the meteoric deposition
25 of ^{10}Be are preserved in sediments and ice cores and can thus be utilized for their synchronization. In this study,
26 for the first time, we use the authigenic $^{10}\text{Be}/^9\text{Be}$ record of a Laptev Sea sediment core for the period 8-14 kyr BP
27 and synchronize it with the ^{10}Be records from absolutely dated ice cores. Based on the resulting absolute
28 chronology, a benthic ΔR value of $+345 \pm 60$ ^{14}C years was estimated for the Laptev Sea, which corresponds to a
29 marine reservoir age of 848 ± 90 ^{14}C years. The ΔR value was used to refine the age-depth model for core PS2458-
30 4, establishing it as a potential reference chronology for the Laptev Sea. We also compare the calculated ΔR value
31 with modern estimates from the literature and discuss its implications for the age-depth model.

32

33 **1 Introduction**

34

35 Paleoclimate reconstructions can provide useful information about the dynamics of the climate system under
36 different boundary conditions. Investigating how the climate variations propagate in space and time can provide
37 important information about the underlying driving mechanisms (Adolphi et al., 2018; Czymzik et al., 2016b, a;
38 Reinig et al., 2021). To correctly assess regional variations and spatio-temporal patterns in climate fluctuations,
39 it is crucial to construct precise chronological frameworks. These frameworks serve as the temporal backbone for
40 establishing correlations between paleoclimate records derived from marine, terrestrial, and ice-core archives.
41 However, uncertainties in chronologies across different paleoclimate records often hinder the precise assessment
42 of paleoclimate dynamics involving multiple records from different sites and archives (Southon, 2002).

43

44 One of the key challenges for constructing precise chronologies in the marine realm is to estimate the regional
45 marine radiocarbon reservoir age correction, especially in polar regions (Alves et al., 2018; Heaton et al., 2023).



46 For constructing an age-depth model using ^{14}C dates of marine samples, it is crucial to include a precise marine
47 reservoir age (MRA). The MRA is the radiocarbon age difference between a marine sample and its contemporary
48 atmosphere (Stuiver et al., 1986). According to the most recent radiocarbon calibration curve, Marine20, the global
49 average marine reservoir age is approximately 500 ^{14}C years during the Holocene period (0 - 11.6 kyr BP) (Heaton
50 et al., 2020). However, regional differences in ocean-atmosphere exchange and internal ocean mixing can result
51 in large regional deviations from this global mean (Heaton et al., 2023). Therefore, the local marine reservoir
52 effect, ΔR was introduced and is defined as the difference between the regional and the modelled global marine
53 reservoir ages (Reimer and Reimer, 2001; Stuiver et al., 1986).

54

55 There is only one study that has provided modern MRA estimates for the Laptev Sea (Bauch et al., 2001). In this
56 study, the MRAs range from 295 ± 45 to 860 ± 55 ^{14}C years, with a mean value of 451 ± 72 ^{14}C years. Estimates
57 for MRA from the early deglaciation (~15 kyr BP) to the Holocene period for creating reliable deglacial
58 chronologies in the Laptev Sea are so far not available.

59

60 In order to provide estimates of the local ΔR back in time the samples must be independently dated by other means
61 than ^{14}C . This can for example be achieved by synchronization to other well-dated archives. Cosmogenic
62 radionuclides such as ^{10}Be and provide such a synchronization tool (Adolphi et al., 2018; Adolphi and Muscheler,
63 2016; Czymzik et al., 2018, 2020; Muscheler et al., 2014; Southon, 2002).

64

65 The cosmogenic radionuclides Beryllium-10 (^{10}Be , half-life = 1.387 ± 0.012 Myr) (Chmeleff et al., 2010;
66 Korschinek et al., 2010) and Carbon-14 (^{14}C , half-life = 5.700 ± 0.03 kyr) (Audi et al., 2003) are mainly produced
67 in Earth's upper atmosphere in a particle cascade that is triggered when galactic cosmic rays interact with atoms
68 in the atmosphere (Lal and Peters, 1967; Dunai and Lifton, 2014). The flux of these cosmic rays reaching Earth
69 is controlled by variations in the heliomagnetic and geomagnetic shielding (Lal and Peters, 1967; Masarik and
70 Beer, 1999) During periods of higher solar activity and/or geomagnetic field strength, production rates of ^{10}Be
71 and ^{14}C are decreased, whereas the production rates are higher during reduced solar activity and/or lower magnetic
72 field strength. The production rates of both cosmogenic radionuclide isotopes co-vary globally due to these
73 external processes.

74

75 Following production in the atmosphere, ^{14}C oxidizes to $^{14}\text{CO}_2$, enters the global carbon cycle and is incorporated
76 in environmental archives such as tree-rings, foraminifera, or speleothems. Annually, gigatons of carbon are
77 exchanged between the Earth's active reservoirs of the atmosphere, biosphere and the ocean, within the global
78 carbon cycle. Carbon is recycled and reused within these reservoirs and some reservoirs such as the deep ocean
79 can take hundreds of years to recycle carbon back to the atmosphere. The resulting heterogenous distribution of
80 radiocarbon among the different reservoirs stress the importance to understand and determine precise reservoir
81 ages.

82

83 In the atmosphere, the production of ^{10}Be in the more stably layered stratosphere is higher than in the troposphere.
84 About 63 % of ^{10}Be is produced in the stratosphere, 30 % in the tropical and subtropical troposphere together and
85 7 % in the polar troposphere (Adolphi et al., 2023; Poluianov et al., 2016). ^{10}Be is adsorbed onto aerosol particles,



86 mixed during about 1-yr residence time in the stratosphere, and is then transported and deposited on Earth's
87 surfaces through wet and dry deposition (Raisbeck et al., 1981; Zheng et al., 2023). The ^{10}Be production rates are
88 highest in the high-latitude stratosphere due to the weaker shielding of the cosmic ray flux by the Earth's magnetic
89 field. However, the highest ^{10}Be fluxes to Earth's surface are recorded in mid-latitudes because of the strong
90 regional exchange between stratosphere and troposphere and high precipitation rates leading to strong aerosol
91 scavenging (Heikkilä et al., 2013). Non-production processes such as variations in mixing, transport and
92 deposition of ^{10}Be and ^{14}C can complicate the reconstruction of cosmogenic radionuclide production rates from
93 paleoenvironmental archives. However, common variations in both cosmogenic radionuclide records are
94 considered to represent the cosmogenic radionuclide production signal, due to their common production
95 mechanism and different chemical behavior (Lal and Peters, 1967; Muscheler et al., 2008). ^{10}Be production rate
96 changes are relatively well-known from independently dated ice-core records (Finkel and Nishiizumi, 1997; Yiou
97 et al., 1997), and this can serve as a synchronization target for other records of ^{10}Be production rate changes.

98
99 In order to obtain reliable records of ^{10}Be -production rate changes from marine sediments, the effects of variable
100 sedimentation rates and particle scavenging must be accounted for, which can be efficiently achieved by
101 measuring authigenic $^{10}\text{Be}/^9\text{Be}$ (Bourles et al. 1989). The stable isotope ^9Be is a trace component in all continental
102 rocks. It is released by weathering of silicate rocks and transported to the ocean mainly by rivers (von
103 Blanckenburg et al., 2015). ^9Be (and to a lesser extent meteoric ^{10}Be) is introduced into the ocean in its dissolved
104 form where it is mixed with dissolved ^{10}Be of ocean water (mainly derived from atmospheric fallout, see above).
105 Since Be is particle reactive in seawater, dissolved $^{10}\text{Be}/^9\text{Be}$ is incorporated in marine authigenic phases as
106 amorphous coating on sediment or it can be preserved in authigenic Fe-Mn oxyhydroxides (von Blanckenburg
107 and Bouchez, 2014). Therefore, in marine sediment the authigenic $^{10}\text{Be}/^9\text{Be}$ ratio reflects the isotope ratio of
108 dissolved Be of the overlying water column at the time of sediment deposition (Bourles et al., 1989; von
109 Blanckenburg and Bouchez, 2014).

110
111 If the riverine input of ^9Be remains relatively constant, ^9Be and ^{10}Be are well-mixed (i.e., at sites >200 km from
112 the coast) (Wittmann et al., 2017), and the mixing of prevalent water-masses does not change, then authigenic
113 $^{10}\text{Be}/^9\text{Be}$ should primarily reflect changes in the cosmogenic production rates of ^{10}Be . In the Arctic Ocean, the
114 spatial patterns of $^{10}\text{Be}/^9\text{Be}$ in the water column are more heterogeneous than most other open ocean settings
115 because of the mixing of Atlantic waters with $^{10}\text{Be}/^9\text{Be}$ values of $5 - 10 \times 10^{-8}$ and Arctic Rivers with $^{10}\text{Be}/^9\text{Be}$
116 values of $0.3 - 1.5 \times 10^{-8}$) (Frank et al., 2009).

117
118 The aim of this study is to explore the use of an authigenic $^{10}\text{Be}/^9\text{Be}$ of a Laptev Sea sediment core for its
119 synchronization to ^{10}Be -records from absolutely dated ice cores. Using this result, we aim to infer the the local
120 marine reservoir effect, ΔR for the Laptev Sea during the deglaciation. This is the first study to exploit variations
121 in ^{10}Be production rates from Arctic marine sediments for stratigraphic purposes.

122
123
124
125
126
127

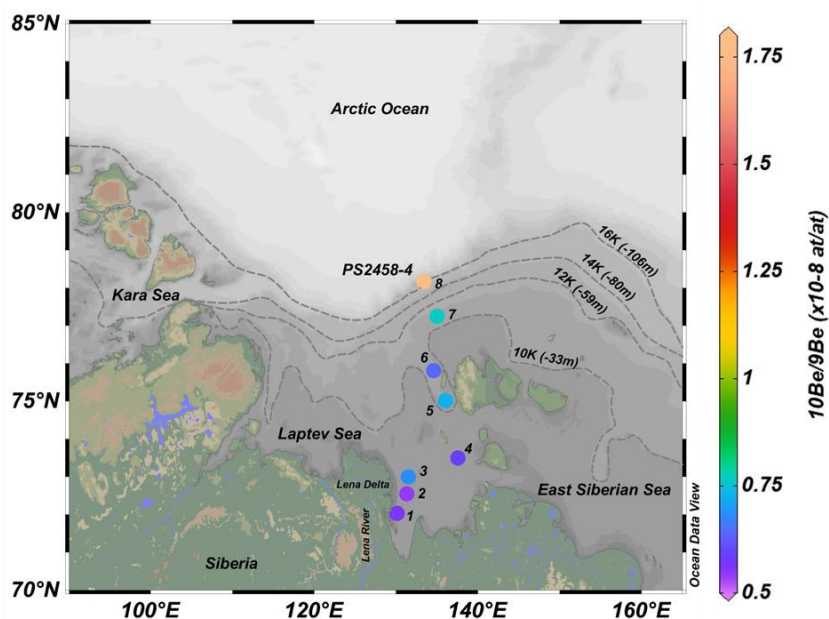


128 **2 Materials and methods**

129 **2.1 Sediment core location and initial chronology**

130 The sediment core PS2458-4 measured for ^9Be and ^{10}Be in this study, was retrieved in 1994 from the eastern
131 Laptev Sea continental margin ($78^\circ 10.0' \text{N}$, $133^\circ 23.9' \text{E}$) at a water depth of 983 m (Fütterer, 1994) and
132 approximately about 518 km from the Lena Delta (Fig. 1). The 8 m long core consists of very dark olive-grey silty
133 clay of dominantly terrigenous origin (Fütterer, 1994). This core consists of a continuous high-sedimentation-rate
134 (77 cm / kyr) sequence representing the deglaciation period between approximately 16.5 and 9.3 kyr BP, followed
135 by a lower-sedimentation-rate (27 cm / kyr) early Holocene sequence (Fahl and Stein, 2012). A first chronology
136 of core PS2458-4 was established by accelerator mass spectrometry (AMS) ^{14}C dating of calcareous foraminifera,
137 bivalves and wood samples for the sediment interval between 201 and 667 cm, corresponding to a time interval
138 between approximately 8.8 and 14.3 kilo-calendar years BP (kyr BP) (Spielhagen et al., 2005). To improve the
139 existing age-depth model, 7 new AMS ^{14}C dates from mixed benthic foraminifera were used in combination with
140 7 ^{14}C dates from mixed benthic foraminifera and bivalves from Spielhagen et al. (2005) and an initial age-model
141 was derived using OxCal4.4 (Ramsey, 2009) (see Table 2). The marine ^{14}C dates were calibrated with the
142 Marine20 curve (Heaton et al., 2020). An average local marine reservoir effect (ΔR) value of -110 ± 28 ^{14}C years
143 was used based on the nearest modern values from Bauch et al. (2001) available from the online database:
144 <http://calib.org/marine/>. This chronology provides the initial basis for the stratigraphic fine-tuning using $^{10}\text{Be}/^9\text{Be}$
145 as described below.

146



147 **Figure 1: Map of the Laptev Sea shelf showing the location of core PS2458-4 with core-top $^{10}\text{Be}/^9\text{Be}$ concentration**
148 **(numbered colored circle 8) and $^{10}\text{Be}/^9\text{Be}$ concentrations of modern surface sediments (numbered colored circles 1-7).**
149 **The dashed lines represent the reconstructed coastline extent at 4 different time periods (where 16K=16 kyr BP) with**
150 **corresponding water depth values in meters shown in brackets (Klemann et al., 2015) . The Map was created using**
151 **Ocean Data View (Schlitzer, 2016)**



152 **2.2 Modern surface sediment samples from Laptev Sea**

153 Seven modern surface sediment samples collected in the Laptev Sea were also included in the analysis (Figure 1,
154 Table 1). Surface sediments with sample IDs 1 to 6 were collected during the Transdrift expeditions I and II in
155 1993 and 1994 using Van Veen grabs and large spade box corer (Kassens and Dmitrenko, 1995; Kassens and
156 Karpiy, 1994). Sediment sample from core PS2728-2 with ID number 7 was recovered in 1995 with a large
157 rectangular box sampler during the Arctic Expedition ARK-XI/1 (Rachor, 1997). The sediment samples used in
158 this study are distributed along a transect from near to the Lena Delta towards the open ocean near the shelf break,
159 close to where core PS2458-4 was retrieved.

160 **2.3 Sample preparation and measurements**

161 Fifty-four sediment samples were selected along core PS2458-4 and processed for Be isotope analysis at the
162 Alfred Wegener Institute in Bremerhaven (Germany). According to the initial radiocarbon-based age model, the
163 selected samples covered three large cosmogenic radionuclide production rate swings, as evidenced by ice core
164 ^{10}Be and tree-ring ^{14}C records (e.g., Adolphi and Muscheler, 2016), that occurred between 8.5 and 11.5 kyr BP.
165 The leaching of the authigenic Fe-Mn oxyhydroxides phase followed Gutjahr et al. (2007) with minor
166 modifications. Sediment samples were freeze-dried, homogenised and ~1 g of sediment was treated with 1 M
167 NaOAc and adjusted with HOAc to pH 4 to dissolve carbonates which were discarded. Subsequently, the
168 sediments were leached using 0.04 M hydroxylamine ($\text{NH}_2\text{OH}\cdot\text{HCl}$) in 15% HOAc at 95 °C for 4 h. We did not
169 leach the exchangeable fraction as proposed by Gutjahr et al. (2007) as this contained less than 1 % of the Be
170 leached in the hydroxylamine fraction with a very similar $^{10}\text{Be}/^9\text{Be}$ ratio. An aliquot from the resulting leaching
171 solution was sampled for stable ^9Be measurements using an Atomic Emission Spectrophotometer at the Alfred
172 Wegener Institute in Bremerhaven, Germany (Thermo Fisher Scientific Inc., ICP-OES-iCAP7400), with an
173 internal Yttrium standard and standard addition. The remaining ^{10}Be aliquot solution was spiked with a precisely
174 weighed amount of ^9Be -carrier (200, 300 or 500 μL of 1000 mg/L carrier solution, LGC 998969-73, $^{10}\text{Be}/^9\text{Be} =$
175 $(3.74 \pm 0.31) \times 10^{-15}$ at/at) (Merchel et al., 2021). The purification of the samples largely followed the method
176 outlined by Simon et al. (2016). The samples were evaporated, dissolved in distilled HCl and NH_3 was added for
177 Be oxy-hydroxide precipitation from the solution at pH 8 - 9. The precipitate was recovered by centrifugation and
178 then dissolved in 1 mL distilled 10.2 M HCl before loading onto a column filled with 15 mL Dowex® 1 x 8 (100-
179 200 mesh) anion-exchange resin in order to remove Fe from the sample. Prior, the resin was rinsed with 20 mL
180 MilliQ® water and conditioned with 30 mL 10.2 M HCl. The sample was then loaded onto the column and eluted
181 using 30 mL 10.2 M HCl. A column filled with 10 mL 50 x 8 (100 - 200 mesh) cation-exchange resin was used to
182 separate Be from B and Al. The resin was treated with 20 mL MilliQ® water followed by 20 mL 1 M HCl. The
183 sample was loaded onto the column and the first 25 mL 1 M HCl eluent, which contain mainly B, were discarded.
184 Be was eluted and collected with the next addition of 90 mL 1 M HCl. The resulting Be oxy-hydroxides were
185 precipitated at pH 8 - 9 by addition of NH_3 , then separated by centrifugation and washed 3 times by rinsing with
186 MilliQ® water to remove all chlorides. The purified Be oxy-hydroxides were transferred into quartz vials, dried
187 at 80 °C overnight and finally calcinated to BeO at 900 °C for 2 h. The BeO was mixed with Nb powder ($\text{Nb}:\text{BeO}$
188 $= 4 : 1$ by weight) and pressed into a Cu cathode-holder for accelerator mass spectrometer (AMS) measurements.
189 One blank and one replicate were measured with each batch of samples in order to assess reproducibility and
190 background during the extraction procedure.



191 AMS measurements were performed at DREAMS (DREsden AMS) facility (Lachner et al., 2023; Rugel et al.,
192 2016). All measurements were done relative to the standard “SMD-Be-12” with a weighted mean value of $(1.704$
193 $\pm 0.030) \times 10^{-12}$ (Akhmadaliev et al., 2013). Authigenic $^{10}\text{Be}/^9\text{Be}$ was calculated from the AMS results, the known
194 amount of carrier, and the measured authigenic ^9Be -concentration from Inductively Coupled Plasma Atomic
195 Emission Spectroscopy (ICP-AES) (see Simon et al., 2016). Considering the recent age of the samples, we did
196 not correct for decay of ^{10}Be . The correction would be in the order of 0.5 % and is an order of magnitude lower
197 than our combined measurement precision.

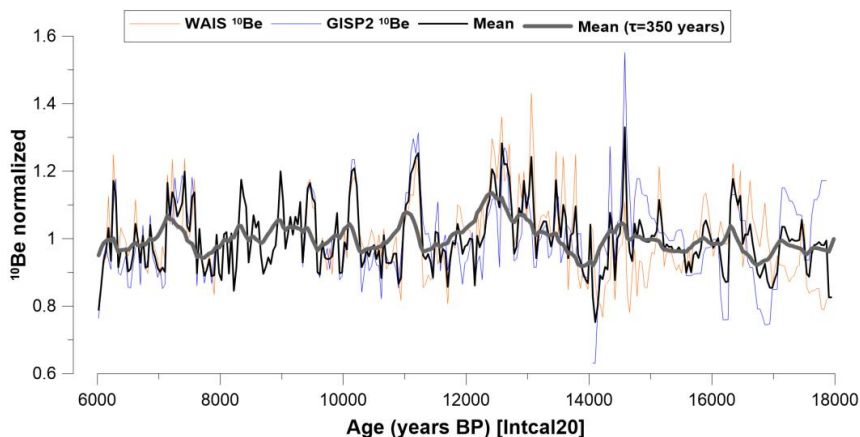
198 The preparation and measurement of the 7 new benthic foraminifera samples were undertaken based on the
199 standard operation procedures routinely used at the MICADAS ^{14}C laboratory facility of the Alfred Wegener
200 Institute (Mollenhauer et al., 2021). Prior to measurement, care was taken to critically select appropriate and
201 sufficient number of foraminifera shells without brownish discolouration or authigenic calcite overgrowth to
202 reduce uncertainty in the radiocarbon dates (Wollenburg et al., 2023).

203 **2.4 Ice core ^{10}Be record**

204 The ice core ^{10}Be record used in this study (Fig. 2) consists of normalized, averaged values of two ice cores: the
205 West Antarctic Ice Sheet (WAIS) Divide ice core ^{10}Be (Muschitiello et al., 2019; Sigl et al., 2016; Sinnl et al.,
206 2023) and the Greenland Ice Sheet Project Two (GISP2) ^{10}Be fluxes (Finkel and Nishiizumi, 1997). The ice core
207 fluxes had been corrected for climate influences by performing a regression against $\delta^{18}\text{O}$ and snow accumulation
208 rates (Adolphi et al., 2018). Prior to averaging, each ice core had been transferred to the IntCal20 timescale using
209 the timescale transfer functions described in several previous studies (Adolphi and Muscheler, 2016; Adolphi et
210 al., 2018 and Sigl et al., 2016). The glacial section of WAIS had been synchronized to Greenland Ice-Core
211 Chronology 2005 (GICC05) by using volcanic (Svensson et al., 2020) and cosmogenic (Sinnl et al., 2023) tie
212 points. The data from each ice core were resampled (averaged) to 40-year resolution before stacking. In order to
213 facilitate a comparison between ice core and marine ^{10}Be changes, we modelled the expected marine signal from
214 the ice core record following Christl (2007). We chose a 350-year residence time of Beryllium in the water column
215 prior to deposition as this leads to a good agreement of amplitudes of the modelled centennial changes in ^{10}Be to
216 the measured $^{10}\text{Be}/^9\text{Be}$ changes seen in the sediment. This 350-year residence time is within the range of values
217 $(80 \pm 5$ to 500 ± 25 years) reported in Arctic Ocean calculated from sedimentary fluxes and inventories (Frank et
218 al., 2009).

219

220



221

222 **Figure 2: WAIS (orange)** (Muschitiello et al., 2019; Sigl et al., 2016; Sinnl et al., 2023) **and GISP2 (blue)** (Finkel and
223 Nishiizumi, 1997) **¹⁰Be fluxes corrected for correlation to ice core accumulation rates and δ¹⁸O, plotted on the IntCal20**
224 **timescale. The thick black line shows the mean of both datasets and the bold grey line depicts the modelled oceanic ¹⁰Be**
225 **signal assuming a residence time (τ) of 350 years for ¹⁰Be in the water column.**

226

227 3 Results

228 The concentrations of ⁹Be, ¹⁰Be and ¹⁰Be/⁹Be atomic ratios from core PS2458-4 are displayed in Fig. 3 and the
229 data are shown in Table S2. The dominant feature is an increasing trend of ¹⁰Be/⁹Be from the bottom to the top of
230 the core. The modern surface sediment ¹⁰Be/⁹Be values $([0.54 - 0.76] \times 10^{-8})$ from the offshore transect spanning
231 from the Lena Delta to the core site (Table 1, Fig. 1) are consistent with ¹⁰Be/⁹Be of Lena water samples $([0.62 \pm$
232 $0.07] \times 10^{-8})$ (Frank et al., 2009) and within the same range as PS2458-4 ¹⁰Be/⁹Be $([0.53 - 1.77] \times 10^{-8})$. They
233 show an increasing trend from the Lena Delta to the open ocean (Fig. 1). The modern values close to the Lena are
234 consistent with the lowest ¹⁰Be/⁹Be values of PS2458-4 during the deglaciation, when the core-site was proximal
235 to the paleo-river mouth of the Lena (see Figure 1).

236 **Table 1. Information about location, water depth, distance from Lena Delta and concentration of**
237 **authigenic ¹⁰Be, ⁹Be, ¹⁰Be/⁹Be ratio leached of the modern surface sediment samples.**

Sample name	Sample ID	Latitude (°)	Longitude (°)	Water Depth (m)	Approx. distance from Lena Delta (km)	⁹ Be (at/g) [x10 ¹⁶]	¹⁰ Be (at/g) [x10 ⁸]	¹⁰ Be/ ⁹ Be (at/at) [x10 ⁻⁸]
IK93Z4-4	1	72.03	130.13	14	28	1.12	0.63	0.56
IK9307-3	2	72.55	131.30	20.7	61	1.60	0.86	0.54
IK9316-6	3	73.00	131.50	27.8	65	1.89	1.15	0.61
IK9318-5	4	73.50	137.55	24	269	1.58	0.92	0.59
IK9350-6	5	75.02	136.03	31	295	1.13	0.82	0.72
IK9373A-6	6	75.81	134.58	46	322	1.46	0.93	0.64
PS2728-2a-1	7	77.25	135.01	44	471	1.42	1.09	0.76
PS2458-4*	8	78.17	133.38	983	518	1.28	1.95	1.77

*For core PS2458-4, the ⁹B, ¹⁰Be and ¹⁰Be/⁹Be results from the 30 cm sample are used as the core-top values.

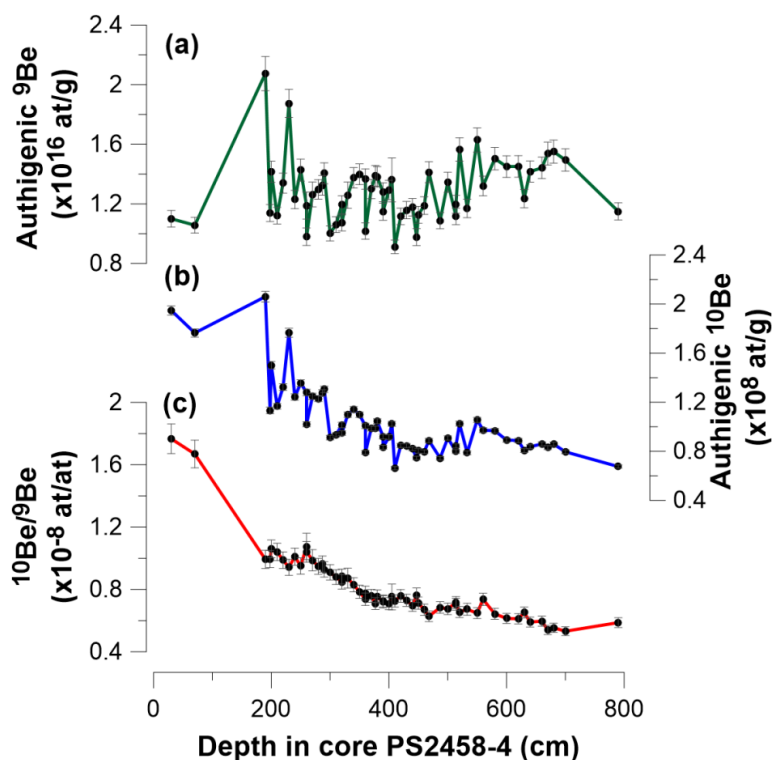
238



239 In order to use $^{10}\text{Be}/^9\text{Be}$ as a synchronization tool, we must remove this influence of mixing riverine and marine
 240 endmembers. It is non-trivial to derive a quantitative end-member mixing model solely from local sea-level
 241 reconstructions because sea-level only provides conceptual evidence about the variable proportions of open ocean
 242 and riverine water masses bathing the core site. Hence, we chose a statistical model, assuming that the changes in
 243 the endmember-mixing were gradual and hence, can be removed by normalizing to the long-term trend in the
 244 $^{10}\text{Be}/^9\text{Be}$ record. The residual centennial variability in $^{10}\text{Be}/^9\text{Be}$ is hypothesized to be driven by ^{10}Be -production
 245 rate changes and therefore suitable for synchronization.

246

247 Three different statistical models were used to test the sensitivity of our results to the choice of detrending
 248 techniques. Figure 4a illustrates the three different trend fitting techniques (logarithmic, power, and LOESS
 249 (LOcally Estimated Scatterplot Smoothing) applied to the $^{10}\text{Be}/^9\text{Be}$ data set. The relative $^{10}\text{Be}/^9\text{Be}$ residuals are
 250 plotted with respect to the logarithmic, power and LOESS trends (Fig. 4b) and the differences fall within the
 251 measurement uncertainties of the individual data points, showing that variations of the $^{10}\text{Be}/^9\text{Be}$ ratio are robust
 252 against the choice of the detrending model.

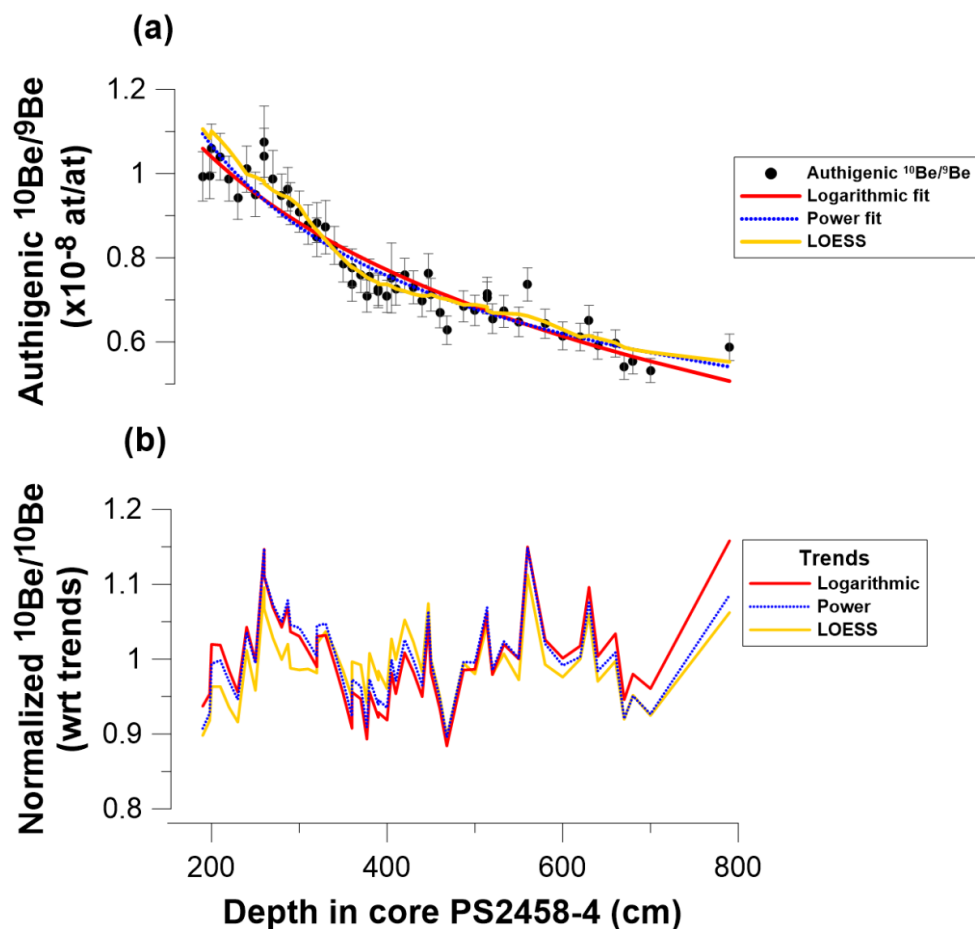


253

254 **Figure 3: Concentrations of (a) ^9Be , (b) ^{10}Be and (c) $^{10}\text{Be}/^9\text{Be}$ atomic ratios from core PS2458-4**

255

256



257

258

259

260

Figure 4: Sensitivity tests (a) Three different trend fitting techniques (logarithmic, power, and LOESS), (b) Relative $^{10}\text{Be}/^9\text{Be}$ residuals with respect to logarithmic, power and LOESS trends

261

262 To check whether the detrended $^{10}\text{Be}/^9\text{Be}$ record is driven by cosmogenic ^{10}Be production rate changes, we
 263 compare the detrended signal to the ice core ^{10}Be -record. Figure 5 shows the ice core ^{10}Be record and PS2458-4
 264 mean profile of the three detrended data sets with a 3-point LOESS graph plotted on an initial ^{14}C -based age-scale
 265 (see used ΔR value below). Note however, that the following analyses have been performed on all three versions
 266 of the detrended dataset in order to test the robustness of our results against the choice of the detrending method.
 267 The variations observed in the sediment $^{10}\text{Be}/^9\text{Be}$ record follow closely the same pattern and relative amplitudes
 268 compared with the ice core ^{10}Be record. Therefore, we suggest that the variations observed in the $^{10}\text{Be}/^9\text{Be}$ record
 269 indeed reflect the production rate changes in the centennial range.

270

271 In order to refine the initial ^{14}C -based chronology and infer a regional deglacial ΔR -estimate, we constructed ^{14}C -
 272 based age-depth-models for PS2458-4 using OxCal 4.4 (Ramsey, 2009) assuming a range of ΔR between -110



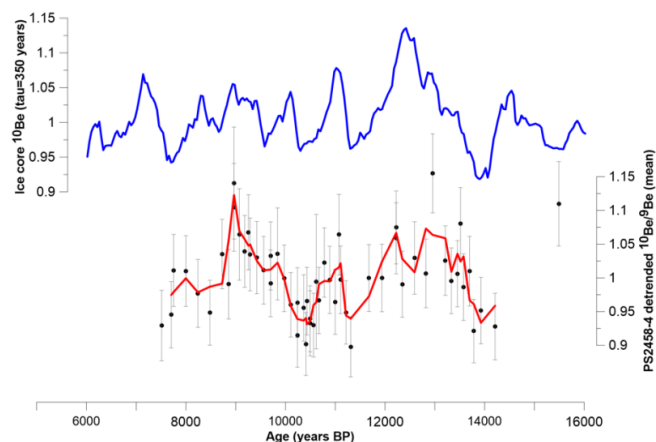
273 (Bauch et al., 2001) and +800 ¹⁴C years. Each age-model was then evaluated by comparing the resulting PS2458-
 274 4 ¹⁰Be/⁹Be-timeseries to the ice core ¹⁰Be-record. For this purpose, we use the generalized likelihood function by
 275 Christen and Pérez, (2009) that is otherwise used for the calibration of ¹⁴C-dates:
 276

$$277 \quad L_{\Delta R} \propto \prod_{j=1}^n \left[b + \frac{(x_j - y(t_j))^2}{2(\sigma_x^2 + \sigma_y^2)} \right]^{-(a+\frac{1}{2})}$$

278
 279 In our case, the ice core provides the calibration that describes ¹⁰Be-anomalies at each point in time (y(t)) which
 280 is compared to the sediment ¹⁰Be/⁹Be (x_j) on their modelled absolute age assuming a certain reservoir age. We use
 281 a = 3 and b = 4 based on the recommendation of Christen and Pérez (2009). This allows us to use ¹⁰Be to compare
 282 the likelihoods of different age models, and thus ¹⁴C-reservoir ages.
 283

284 The likelihood values were calculated for each of the three different trend fitting techniques and are shown in
 285 Figure 6. They result in a mean ΔR ± 1σ of 360 ± 75, 340 ± 50 and 335 ± 55 ¹⁴C years for the logarithmic, power
 286 and LOESS trend fitting techniques, respectively. These values are statistically indistinguishable and hence, we
 287 opt for the arithmetic mean ΔR value of 345 ± 60 ¹⁴C years. By using a global average marine reservoir age of
 288 503 ± 63 ¹⁴C years for the period 7.51-14.21 kyr BP (Heaton et al., 2020), we estimated a local MRA of 848 ± 90
 289 ¹⁴C years for the Laptev Sea during the deglaciation. The age-depth model for core PS2458-4 was reconstructed
 290 using radiocarbon dates of mixed benthic bivalves and benthic foraminifera (Spielhagen et al., 2005). Therefore,
 291 our calculated ΔR and corresponding MRA reflects to a benthic value.
 292

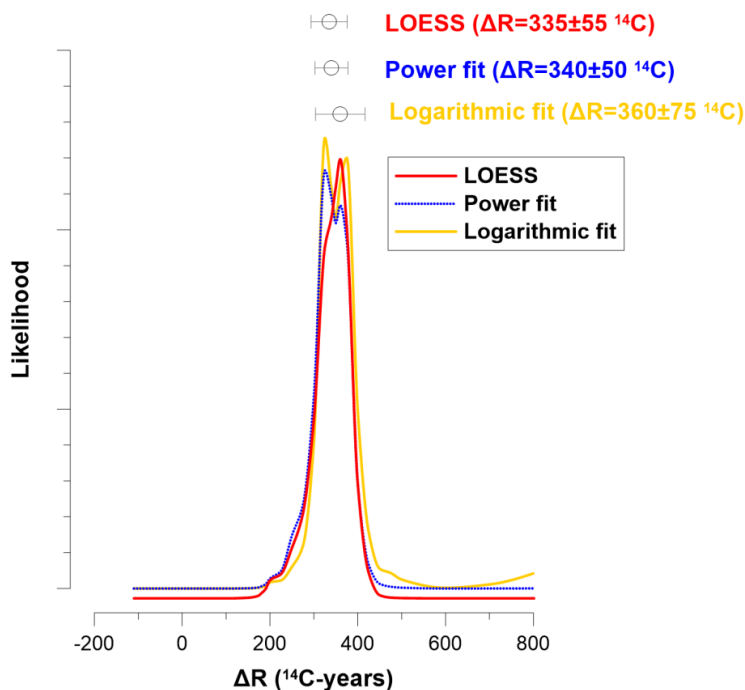
293 The depositional age-depth model with a ΔR value of 345 ± 60 ¹⁴C years for core PS2458-4 is shown in Figure
 294 S2 in the Supplement accompanying this manuscript. Compared to the mean modelled ages calculated with a ΔR
 295 value of -110 ± 28 ¹⁴C years, the new modelled ages computed with a ΔR value of 345 ± 60 ¹⁴C years were
 296 observed to shift younger in the range of 429 to 707 years (Table S1).



297
 298 **Figure 5: Ice core ¹⁰Be record with tau=350 years (blue) and PS2458-4 record calculated from the mean of the three**
 299 **detrended data sets with a 3-point LOESS graph using ΔR value of 345±60 ¹⁴C years for age-model (red)**



300



301

302

Figure 6: Likelihood results with mean $\Delta R \pm 1\sigma$ values of 360 ± 75 , 340 ± 50 and 335 ± 55 ^{14}C years BP based on LOESS (red), power (blue dotted) and logarithmic (yellow) trend fitting techniques respectively.

303

304

305

Table 2. Radiocarbon and modelled ages from foraminifera and bivalve samples from core PS2458-4

Depth (cm)	Sample ID	^{14}C Age (^{14}C years)	\pm (years)	Modelled Age (mean) (cal BP)	Modelled Age (cal BP, 2σ)	Sample type
667	KIA6113	12600	110	13745	14089 – 13360	mixed bivalves, benthic forams
578	AAR-3087	12270	65	13198	13428 – 12982	mixed benthic forams
530	AAR-3086	11560	100	12551	12815 – 12244	mixed benthic forams
491*	AWI-7415.1.1	10968	159	11753	12220 – 11280	mixed benthic forams
467	AAR-3085	10600	75	11291	11630 – 11005	mixed benthic forams
399	AAR-3084	10090	65	10551	10811 – 10276	mixed benthic forams
369	AAR-3083	10020	70	10357	10606 – 10135	mixed benthic forams
331.5*	AWI-7412.1.1	9596	122	9860	10183 – 9527	mixed benthic forams
291.5*	AWI-7411.1.1	9089	224	9305	9711 – 8917	mixed benthic forams
252	AAR-3082	8830	55	8880	9129 – 8615	mixed benthic forams
241.5*	AWI-7410.1.1	8762	141	8762	9058 – 8448	mixed benthic forams
141.5*	AWI-7409.1.1	6447	158	6334	6696 – 5969	mixed benthic forams
121.5*	AWI-7408.1.1	6029	134	5985	6297 – 5638	mixed benthic forams
0.5*	AWI-7786.3.1	0		0		mixed benthic forams

Modelled ages were calculated using OxCal4.4 (Ramsey, 2009) with a ΔR value of 345 ± 60 ^{14}C years BP, as calculated in this study. Marine ^{14}C dates were calibrated with the Marine20 curve (Heaton et al., 2020). The depth values with asterisks represent the new benthic foraminifera samples measured for ^{14}C dates. The depth values without asterisks show the ^{14}C dates published ^{14}C dates from Spielhagen et al. (2005).

306

307



308 **4 Discussion**

309 We have been able to quantitatively compare the agreement between ice core ^{10}Be and sediment $^{10}\text{Be}/^9\text{Be}$ for
310 different ΔR values and visually, we can observe how the two records representing cosmogenic radionuclide
311 production variations are in-phase with each other. It is a more robust approach to compare whole timeseries by
312 using a statistical method such as the likelihood function, instead of matching single wiggles with each other from
313 both records. The latter method is more prone to noise in each dataset and complicates the correct identification
314 of matching peaks.

315

316 When modelling the ice core data, we have assumed a 350-year residence time of ^{10}Be in the water column prior
317 to deposition. We tested the influence of choosing different residence times of ^{10}Be in the water column when
318 modelling the ice core data and then synchronizing the modeled data sets with the PS2458-4 $^{10}\text{Be}/^9\text{Be}$ -timeseries.
319 Different tau values ($\tau = 200, 500, 600$ years) were used to model the ice core data and the ΔR -likelihood values
320 from the LOESS-smoothed ^{10}Be record were calculated. We observed that for all assumed tau-values likelihood
321 peaks occur at a ΔR value of 360 ^{14}C years (Fig. 7). This indicates that the most likely ΔR value is not strongly
322 dependent on the different assumed tau values. We found that only for the tau value of 200 years another best
323 likelihood estimate occurs at a ΔR value of 300 ^{14}C years BP, followed by the secondary likelihood maximum at
324 a ΔR value of 360 ^{14}C years BP. Figure S2 shows the modelled ice core time series with a tau value of 200 years,
325 which indicates clearly larger ^{10}Be amplitudes than what was calculated with a tau value of 350 years, which are
326 larger than the $^{10}\text{Be}/^9\text{Be}$ changes seen in PS2458-4. Based on these results, it seems unlikely that the best likelihood
327 estimate occurring at a ΔR value of 300 ^{14}C years BP with tau=200 years is real.

328

329 Our calculated local benthic MRA value of 848 ± 90 ^{14}C years BP is consistent with the modern values calculated
330 by Bauch et al. (2001), which range from 295 ± 45 to 860 ± 55 ^{14}C years. The largest modern reservoir age of 860
331 ± 55 ^{14}C years is located closest to the Lena Delta, which is comparable to the setting of the location of core
332 PS2458-4 during deglaciation around 14 - 12 kyr BP. Another study from the central Arctic Ocean reported MRA
333 values of 1400 ^{14}C years BP ($\Delta R = 1000$) during the Late Glacial and 700 ^{14}C years BP ($\Delta R = 300$) during the
334 Holocene (Hanslik et al., 2010).

335

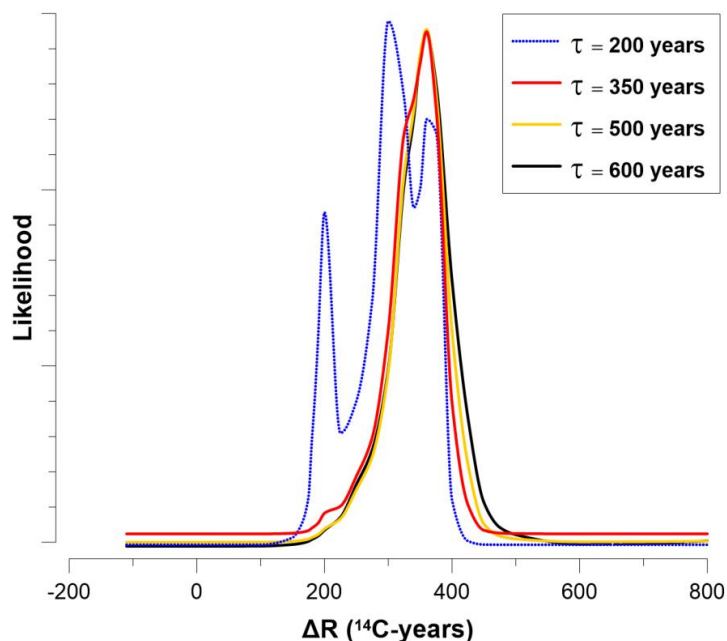
336 The ΔR value was calculated during the deglaciation (14-8 kyr BP) and during this period the mean relative sea
337 level rose by about 64 m (Klemann et al., 2015). The core was retrieved at a depth of 983 m in 1994 and at 14 and
338 8 kyr BP the depths were about 903 and 967 m respectively. Moreover, as shown in Figure 1, the modern surface
339 $^{10}\text{Be}/^9\text{Be}$ values show an increasing trend from the Lena Delta to the open ocean (Fig. 1). Thus, we attribute the
340 trend in PS2458-4 $^{10}\text{Be}/^9\text{Be}$ to deglacial sea level rise and the associated coastline retreat (Bauch et al., 2001;
341 Klemann et al., 2015). During the glacial period, the core site was located close to the Lena River mouth and
342 hence, bathed in river-water with low $^{10}\text{Be}/^9\text{Be}$. With increasing sea-level and coastline retreat, open ocean waters
343 with higher $^{10}\text{Be}/^9\text{Be}$ became more dominant.

344

345

346

347



348

349 **Figure 7. Likelihood results based on different ΔR for the LOESS-smoothed ice core ^{10}Be using for different tau values**
 350 **of 200, 350, 500 and 600 years.**

351

352 We compared our estimated ΔR value 345 ± 60 ^{14}C years with the approach proposed by Heaton et al. (2023) to
 353 infer glacial ΔR values in polar regions. In the polar regions (outside $40^\circ \text{S} - 40^\circ \text{N}$), it is expected that during
 354 glacial episodes, there may have been regional differences in the amount of oceanic ^{14}C depletion compared to
 355 the global non-polar ocean mean represented by Marine20. The increase in the volume and density of sea ice
 356 limiting air-sea gas-exchange may cause a significant larger ΔR during the glacial era compared to the interglacial
 357 values. For glacial periods (55.0 - 11.5 kyr BP), Heaton et al. (2023) proposed a latitude-dependent method to
 358 infer upper bounds of the possible ΔR difference between Holocene and Glacial in polar regions. A lower bound
 359 ΔR^{Hol} is based on samples from the Holocene and an upper (glacial) bound ΔR^{GS} , is calculated by increasing ΔR^{Hol}
 360 depending on the latitude.

361

362 The PS2458-4 record used in this study extends from about 7.5 to 14.2 kyr BP and therefore covers the early
 363 Holocene and parts of the deglacial period. Thus, from 11.5 to 14.2 kyr BP, the record extends into the glacial and
 364 samples from this period may require a glacial polar boost as proposed by Heaton et al. (2023). We calculated
 365 ΔR^{Hol} from ^{14}C samples found in the online database at <http://calib.org/marine/> (Reimer and Reimer, 2001). Using
 366 the weighed mean value of the 5 nearest ΔR values from the core location in the Laptev Sea from Bauch et al.
 367 (2001), yields a ΔR^{Hol} value of -95 ± 61 ^{14}C years. ΔR^{GS} was calculated as: $\Delta R^{\text{GS}} = \Delta R^{\text{Hol}} + \Delta R^{\text{Hol} \rightarrow \text{GS}}$, in agreement
 368 with the GS scenario as described in Heaton et al. (2023). The value $\Delta R^{\text{Hol} \rightarrow \text{GS}}$ is dependent on the latitude of the



369 sample and at 78.75 °N, it amounts to 790 ¹⁴C years. The resulting ΔR^{GS} value is 695 ± 61 ¹⁴C years and is much
370 larger than our inferred benthic ΔR value (345 ± 60 ¹⁴C years).

371

372 These differences are likely due to distinct regional changes in climate and hydrology. At the core location in the
373 Laptev Sea, sea-ice cover was less during the Younger Dryas and Heinrich Stadial 1 compared to the Holocene
374 (Fahl and Stein, 2012), contrary to large-scale deglacial sea ice trends included in the model by Heaton et al.
375 (2023). The expansion of regional sea-ice cover during the recent past in the Laptev Sea could have further
376 influenced the ΔR value, which then should have been larger during the Holocene compared to the early
377 deglaciation. However, our calculated ΔR value of 345 ± 60 ¹⁴C years is larger than the modern average ΔR value
378 of -95 ± 61 ¹⁴C years, making it unlikely that sea-ice cover dynamics were the main driver of past changes in
379 regional ΔR . Instead, as mentioned before, the local reservoir ages in the region are spatially highly variable and
380 influenced by a hardwater effect (Bauch et al. 2001). These regional processes are thus site specific and hence,
381 obviously cannot be covered by the approach of Heaton et al. (2023). Bauch et al. (2001) reported that the
382 relatively old ¹⁴C-age of bivalve shells collected in proximity of the Lena Delta near Tiksi Bay, might be due to
383 the influence of local hardwater effect. This is consistent with the modern setting where the largest ΔR is found
384 close to the Lena Delta and lower ΔR towards the shelf-edge (Bauch et al., 2001). Hence, the larger deglacial ΔR
385 of PS2458-4 could be driven by its proximity to the Lena River during that time as evidenced by low ¹⁰Be/⁹Be as
386 discussed earlier.

387

388

389 **5 Conclusion**

390 We present high-resolution ⁹Be and ¹⁰Be records reconstructed from core PS2458-4, which was retrieved from the
391 continental slope of the eastern Laptev Sea in the Arctic Ocean. We demonstrate that these records are influenced
392 by the distance of the core site to the Lena River, which changed depending on sea-level. Centennial to millennial
393 scale variability in the ¹⁰Be/⁹Be ratio can be attributed to variations in production rate and can hence be used to
394 correlate our sediment record to ice-core ¹⁰Be records.

395

396 This is the first study to reconstruct high-resolution ¹⁰Be production rate changes from ¹⁰Be/⁹Be records from
397 Arctic marine sediments for correlation to ice cores, and this approach has been applied with success. We have
398 correlated the ¹⁰Be from marine sediment core PS2458-4 with ¹⁰Be from ice core and used a likelihood function
399 to estimate ΔR values.

400

401 Our estimate for the deglacial benthic ΔR value for the Laptev Sea is 345 ± 60 ¹⁴C years BP corresponding to a
402 MRA of 848 ± 90 ¹⁴C years. The ΔR value will be used to refine the age-depth model for core PS2458-4 from the
403 Laptev Sea, which could be used as a reference chronology for the Laptev Sea.

404

405 **Data availability**

406

407 The ⁹Be, ¹⁰Be and ¹⁰Be/⁹Be data sets from core PS2458-4 generated in this study are available as a Supplement
408 to this paper.

409



410 **Author contributions**

411

412 FA and GM designed the study. AN, MM conducted the laboratory analyses and FA, AN and GM analyzed the
413 data. JL and KS were responsible for preparation and conduction of the ¹⁰Be AMS measurements. JW selected
414 appropriate foraminifera samples for radiocarbon dating. HG undertook the radiocarbon measurement of the
415 foraminifera samples and analyzed the data. AN drafted a first version of the paper and FA and AN generated the
416 figures. All co-authors contributed to the writing and provided feedback on the paper.

417

418 **Competing interests**

419

420 The contact author has declared that neither of the authors has any competing interests.

421

422

423 **Acknowledgements**

424

425 Parts of this research were carried out at the Ion Beam Centre (IBC) at the Helmholtz-Zentrum Dresden-
426 Rossendorf e. V., a member of the Helmholtz Association. We would like to thank the DREAMS operator team
427 for their assistance with AMS-measurements. FA was supported by the Helmholtz Association (VH-NG 1501).
428 We are grateful for the technical support offered by Torben Gentz and Elizabeth Bonk from the MICADAS facility
429 at AWI Bremerhaven. AN would like to thank DAAD and POLMAR for support during his doctoral studies.

430

431

432

433

434

435

436

437

438

439

440

441

442

443

444

445

446

447

448

449

450

451

452

453

454

455

456

457



458 **References**

- 459 Adolphi, F. and Muscheler, R.: Synchronizing the Greenland ice core and radiocarbon timescales over
460 the Holocene-Bayesian wiggle-matching of cosmogenic radionuclide records, *Climate of the Past*, 12,
461 15–30, <https://doi.org/10.5194/cp-12-15-2016>, 2016.
- 462 Adolphi, F., Bronk Ramsey, C., Erhardt, T., Edwards, R. L., Cheng, H., Turney, C. S. M., Cooper, A.,
463 Svensson, A., Rasmussen, S. O., Fischer, H., and Muscheler, R.: Connecting the Greenland ice-core
464 and U/Th timescales via cosmogenic radionuclides: testing the synchronicity of Dansgaard–Oeschger
465 events, *Climate of the Past*, 14, 1755–1781, <https://doi.org/10.5194/cp-14-1755-2018>, 2018.
- 466 Adolphi, F., Herbst, K., Nilsson, A., and Panovska, S.: On the Polar Bias in Ice Core ^{10}Be Data, *Journal*
467 *of Geophysical Research: Atmospheres*, 128, <https://doi.org/10.1029/2022JD038203>, 2023.
- 468 Akhmadaliev, S., Heller, R., Hanf, D., Rugel, G., and Merchel, S.: The new 6MV AMS-facility
469 DREAMS at Dresden, *Nucl Instrum Methods Phys Res B*, 294, 5–10,
470 <https://doi.org/10.1016/j.nimb.2012.01.053>, 2013.
- 471 Alves, E. Q., Macario, K., Ascough, P., and Bronk Ramsey, C.: The Worldwide Marine Radiocarbon
472 Reservoir Effect: Definitions, Mechanisms, and Prospects, *Reviews of Geophysics*, 56, 278–305,
473 <https://doi.org/https://doi.org/10.1002/2017RG000588>, 2018.
- 474 Audi, G., Bersillon, O., Blachot, J., and Wapstra, A. H.: The NUBASE evaluation of nuclear and decay
475 properties, *Nucl Phys A*, 729, <https://doi.org/10.1016/j.nuclphysa.2003.11.001>, 2003.
- 476 Bauch, H. A., Mueller-Lupp, T., Taldenkova, E., Spielhagen, R. F., Kassens, H., Grootes, P. M., Thiede,
477 J., Heinemeier, J., and Petryashov, V. V.: Chronology of the holocene transgression at the north
478 siberian margin, *Glob Planet Change*, 31, [https://doi.org/10.1016/S0921-8181\(01\)00116-3](https://doi.org/10.1016/S0921-8181(01)00116-3), 2001.
- 479 Von Blanckenburg, F. and Bouchez, J.: River fluxes to the sea from the ocean’s $^{10}\text{Be}/^{9}\text{Be}$ ratio, *Earth*
480 *Planet Sci Lett*, 387, 34–43, <https://doi.org/10.1016/j.epsl.2013.11.004>, 2014.
- 481 von Blanckenburg, F., Bouchez, J., Ibarra, D. E., and Maher, K.: Stable runoff and weathering fluxes into
482 the oceans over Quaternary climate cycles, *Nat Geosci*, 8, 538–542, <https://doi.org/10.1038/ngeo2452>,
483 2015.
- 484 Bourles, D., Raisbeck, G. M., and Yiou, F.: ^{10}Be and ^{9}Be in marine sediments and their potential for
485 dating, 443–452 pp., 1989.
- 486 Chmeleff, J., von Blanckenburg, F., Kossert, K., and Jakob, D.: Determination of the ^{10}Be half-life by
487 multicollector ICP-MS and liquid scintillation counting, *Nucl Instrum Methods Phys Res B*, 268,
488 192–199, <https://doi.org/10.1016/j.nimb.2009.09.012>, 2010.
- 489 Christen, A. J. and Pérez, S. E.: A new robust statistical model for radiocarbon data, *Radiocarbon*, 51,
490 <https://doi.org/10.1017/s003382220003410x>, 2009.
- 491 Christl, M.: Sensitivity and response of beryllium-10 in marine sediments to rapid production changes
492 (geomagnetic events): A box model study, *Geochemistry, Geophysics, Geosystems*, 8,
493 <https://doi.org/10.1029/2007GC001598>, 2007.
- 494 Czymzik, M., Dreibrodt, S., Feeser, I., Adolphi, F., and Brauer, A.: Mid-Holocene humid periods
495 reconstructed from calcite varves of the Lake Woserin sediment record (north-eastern Germany),
496 *Holocene*, 26, 935–946, <https://doi.org/10.1177/0959683615622549>, 2016a.
- 497 Czymzik, M., Muscheler, R., and Brauer, A.: Solar modulation of flood frequency in central Europe
498 during spring and summer on interannual to multi-centennial timescales, *Climate of the Past*, 12, 799–
499 805, <https://doi.org/10.5194/cp-12-799-2016>, 2016b.
- 500 Czymzik, M., Muscheler, R., Adolphi, F., Mekhaldi, F., Dräger, N., Ott, F., Slowinski, M., Blaszkiewicz,
501 M., Aldahan, A., Possnert, G., and Brauer, A.: Synchronizing ^{10}Be in two varved lake sediment
502 records to IntCal13 ^{14}C during three grand solar minima, *Climate of the Past*, 14, 687–696,
503 <https://doi.org/10.5194/cp-14-687-2018>, 2018.
- 504 Czymzik, M., Nowaczyk, N. R., Dellwig, O., Wegwerth, A., Muscheler, R., Christl, M., and Arz, H. W.:
505 Lagged atmospheric circulation response in the Black Sea region to Greenland Interstadial 10,
506 <https://doi.org/10.1073/pnas.2005520117/-/DCSupplemental>, 2020.
- 507 Dunai, T. J. and Lifton, N. A.: The nuts and bolts of cosmogenic nuclide production, *Elements*, 10, 347–
508 350, <https://doi.org/10.2113/gselements.10.5.347>, 2014.
- 509 Fahl, K. and Stein, R.: Modern seasonal variability and deglacial/Holocene change of central Arctic
510 Ocean sea-ice cover: New insights from biomarker proxy records, *Earth Planet Sci Lett*, 351–352,
511 123–133, <https://doi.org/10.1016/j.epsl.2012.07.009>, 2012.



- 512 Finkel, R. C. and Nishiizumi, K.: Beryllium 10 concentrations in the Greenland Ice Sheet Project 2 ice
513 core from 3-40 ka, *J Geophys Res Oceans*, 102, <https://doi.org/10.1029/97JC01282>, 1997.
- 514 Frank, M., Porcelli, D., Andersson, P., Baskaran, M., Björck, G., Kubik, P. W., Hattendorf, B., and
515 Guenther, D.: The dissolved Beryllium isotope composition of the Arctic Ocean, *Geochim
516 Cosmochim Acta*, 73, <https://doi.org/10.1016/j.gca.2009.07.010>, 2009.
- 517 Fütterer, D. K.: The expedition ARCTIC'93, Leg ARK-IX/4 of RV "Polarstern" 1993, Report on Polar
518 Research, 149, 244pp., 1994.
- 519 Gutjahr, M., Frank, M., Stirling, C. H., Klemm, V., van de Flierdt, T., and Halliday, A. N.: Reliable
520 extraction of a deepwater trace metal isotope signal from Fe-Mn oxyhydroxide coatings of marine
521 sediments, *Chem Geol*, 242, 351–370, <https://doi.org/10.1016/j.chemgeo.2007.03.021>, 2007.
- 522 Hanslik, D., Jakobsson, M., Backman, J., Björck, S., Sellén, E., O'Regan, M., Fornaciari, E., and Skog,
523 G.: Quaternary Arctic Ocean sea ice variations and radiocarbon reservoir age corrections, *Quat Sci
524 Rev*, 29, <https://doi.org/10.1016/j.quascirev.2010.06.011>, 2010.
- 525 Heaton, T. J., Köhler, P., Butzin, M., Bard, E., Reimer, R. W., Austin, W. E. N., Bronk Ramsey, C.,
526 Grootes, P. M., Hughen, K. A., Kromer, B., Reimer, P. J., Adkins, J., Burke, A., Cook, M. S., Olsen, J.,
527 and Skinner, L. C.: Marine20 - The Marine Radiocarbon Age Calibration Curve (0-55,000 cal BP),
528 *Radiocarbon*, 62, <https://doi.org/10.1017/RDC.2020.68>, 2020.
- 529 Heaton, T. J., Butzin, M., Bard, E., Bronk Ramsey, C., Hughen, K. A., Kohler, P., and Reimer, P. J.:
530 Marine radiocarbon calibration in polar regions: A simple approximate approach using marine20,
531 *Radiocarbon*, 65, <https://doi.org/10.1017/RDC.2023.42>, 2023.
- 532 Heikkilä, U., Beer, J., Abreu, J. A., and Steinhilber, F.: On the atmospheric transport and deposition of
533 the cosmogenic radionuclides (^{10}Be): A review, <https://doi.org/10.1007/s11214-011-9838-0>, June
534 2013.
- 535 Kassens, H. and Dmitrenko, I.: Russian-German Cooperation: The TRANSDRIFT II expedition to the
536 Laptev Sea., Reports on Polar Research , 182, 1–180, 1995.
- 537 Kassens, H. and Karpiv, V. Y.: Russian–German cooperation: the transdrift I expedition to the Laptev
538 sea., Reports on Polar Research, 151–168, 1994.
- 539 Klemann, V., Heim, B., Bauch, H. A., Wetterich, S., and Opel, T.: Sea-level evolution of the Laptev Sea
540 and the East Siberian Sea since the last glacial maximum, *arktos*, 1, [https://doi.org/10.1007/s41063-
541 015-0004-x](https://doi.org/10.1007/s41063-015-0004-x), 2015.
- 542 Korschinek, G., Bergmaier, A., Faestermann, T., Gerstmann, U. C., Knie, K., Rugel, G., Wallner, A.,
543 Dillmann, I., Dollinger, G., von Gostomski, C. L., Kossert, K., Maiti, M., Poutivtsev, M., and
544 Rimmert, A.: A new value for the half-life of ^{10}Be by Heavy-Ion Elastic Recoil Detection and liquid
545 scintillation counting, *Nucl Instrum Methods Phys Res B*, 268, 187–191,
546 <https://doi.org/10.1016/j.nimb.2009.09.020>, 2010.
- 547 Lachner, J., Rugel, G., Vivo Vilches, C., Koll, D., Stübner, K., Winkler, S., and Wallner, A.:
548 Optimization of ^{10}Be measurements at the 6 MV AMS facility DREAMS, *Nucl Instrum Methods
549 Phys Res B*, 535, 29–33, <https://doi.org/10.1016/j.nimb.2022.11.008>, 2023.
- 550 Lal, D. and Peters, B.: Cosmic Ray Produced Radioactivity on the Earth. In: *Handbuch der Physik*, vol.
551 XLVI/2. Springer, New York, 551–612 pp., 1967.
- 552 Masarik, J. and Beer, J.: Simulation of particle fluxes and cosmogenic nuclide production in the Earth's
553 atmosphere, *Journal of Geophysical Research Atmospheres*, 104,
554 <https://doi.org/10.1029/1998JD200091>, 1999.
- 555 Merchel, S., Braucher, R., Lachner, J., and Rugel, G.: Which is the best ^{9}Be carrier for $^{10}\text{Be}/^{9}\text{Be}$
556 accelerator mass spectrometry?, *MethodsX*, 8, <https://doi.org/10.1016/j.mex.2021.101486>, 2021.
- 557 Mollenhauer, G., Grotheer, H., Gentz, T., Bonk, E., and Hefter, J.: Standard operation procedures and
558 performance of the MICADAS radiocarbon laboratory at Alfred Wegener Institute (AWI), Germany,
559 *Nucl Instrum Methods Phys Res B*, 496, <https://doi.org/10.1016/j.nimb.2021.03.016>, 2021.
- 560 Muscheler, R., Kromer, B., Björck, S., Svensson, A., Friedrich, M., Kaiser, K. F., and Southon, J.: Tree
561 rings and ice cores reveal ^{14}C calibration uncertainties during the Younger Dryas, *Nat Geosci*, 1,
562 <https://doi.org/10.1038/ngeo128>, 2008.
- 563 Muscheler, R., Adolphi, F., and Knudsen, M. F.: Assessing the differences between the IntCal and
564 Greenland ice-core time scales for the last 14,000 years via the common cosmogenic radionuclide
565 variations, *Quat Sci Rev*, 106, 81–87, <https://doi.org/10.1016/j.quascirev.2014.08.017>, 2014.



- 566 Muschitiello, F., D’Andrea, W. J., Schmittner, A., Heaton, T. J., Balascio, N. L., deRoberts, N., Caffee,
567 M. W., Woodruff, T. E., Welten, K. C., Skinner, L. C., Simon, M. H., and Dokken, T. M.: Deep-water
568 circulation changes lead North Atlantic climate during deglaciation, *Nat Commun*, 10,
569 <https://doi.org/10.1038/s41467-019-09237-3>, 2019.
- 570 Poluianov, S. V., Kovaltsov, G. A., Mishev, A. L., and Usoskin, I. G.: Production of cosmogenic isotopes
571 ^7Be , ^{10}Be , ^{14}C , ^{22}Na , and ^{36}Cl in the atmosphere: Altitudinal profiles of yield functions, *J Geophys*
572 *Res*, 121, <https://doi.org/10.1002/2016JD025034>, 2016.
- 573 Rachor, E.: Scientific cruise report of the Arctic expedition ARK-XI/1 of RV “Polarstern” in 1995,
574 *Reports on Polar and Marine Research*, 226, 1–336, 1997.
- 575 Raisbeck, G. M., Yiou, F., Fruneau, M., Loiseaux, J. M., Lieuvin, M., and Ravel, J. C.: Cosmogenic
576 $^{10}\text{Be}/^7\text{Be}$ as a probe of atmospheric transport processes, *Geophys Res Lett*, 8, 1015–1018,
577 <https://doi.org/10.1029/GL008i009p01015>, 1981.
- 578 Ramsey, C. B.: Bayesian analysis of radiocarbon dates, *Radiocarbon*, 51,
579 <https://doi.org/10.1017/s0033822200033865>, 2009.
- 580 Reimer, P. J. and Reimer, R. W.: A marine reservoir correction database and on-line interface,
581 *Radiocarbon*, 43, <https://doi.org/10.1017/s0033822200038339>, 2001.
- 582 Reinig, F., Wacker, L., Jöris, O., Oppenheimer, C., Guidobaldi, G., Nievergelt, D., Adolphi, F.,
583 Cherubini, P., Engels, S., Esper, J., Land, A., Lane, C., Pfanzer, H., Remmele, S., Sigl, M., Sookdeo, A.,
584 and Büntgen, U.: Precise date for the Laacher See eruption synchronizes the Younger Dryas, *Nature*,
585 595, <https://doi.org/10.1038/s41586-021-03608-x>, 2021.
- 586 Rugel, G., Pavetich, S., Akhmadaliev, S., Enamorado Baez, S. M., Scharf, A., Ziegenrücker, R., and
587 Merchel, S.: The first four years of the AMS-facility DREAMS: Status and developments for more
588 accurate radionuclide data, *Nucl Instrum Methods Phys Res B*, 370, 94–100,
589 <https://doi.org/10.1016/j.nimb.2016.01.012>, 2016.
- 590 Schlitzer, R.: Ocean Data View, <https://odv.awi.de>, 2016.
- 591 Sigl, M., Fudge, T. J., Winstrup, M., Cole-Dai, J., Ferris, D., McConnell, J. R., Taylor, K. C., Welten, K.
592 C., Woodruff, T. E., Adolphi, F., Bisiaux, M., Brook, E. J., Buizert, C., Caffee, M. W., Dunbar, N. W.,
593 Edwards, R., Geng, L., Iverson, N., Koffman, B., Layman, L., Maselli, O. J., McGwire, K.,
594 Muscheler, R., Nishiizumi, K., Pasteris, D. R., Rhodes, R. H., and Sowers, T. A.: The WAIS Divide
595 deep ice core WD2014 chronology – Part 2: Annual-layer counting (0–31 ka BP), *Climate of the Past*,
596 12, 769–786, <https://doi.org/10.5194/cp-12-769-2016>, 2016.
- 597 Simon, Q., Thouveny, N., Bourlès, D. L., Nuttin, L., Hillaire-Marcel, C., and St-Onge, G.: Authigenic
598 $^{10}\text{Be}/^9\text{Be}$ ratios and ^{10}Be -fluxes (^{230}Th -normalized) in central Baffin Bay sediments during the
599 last glacial cycle: Paleoenvironmental implications, *Quat Sci Rev*, 140, 142–162,
600 <https://doi.org/10.1016/j.quascirev.2016.03.027>, 2016.
- 601 Simml, G., Adolphi, F., Christl, M., Welten, K. C., Woodruff, T., Caffee, M., Svensson, A., Muscheler, R.,
602 and Rasmussen, S. O.: Synchronizing ice-core and U/Th timescales in the Last Glacial Maximum
603 using Hulu Cave ^{14}C and new ^{10}Be measurements from Greenland and Antarctica, *Climate of the*
604 *Past*, 19, <https://doi.org/10.5194/cp-19-1153-2023>, 2023.
- 605 Southon, J.: A first step to reconciling the GRIP and GISP2 Ice-core chronologies, 0-14, 500 yr B.P.,
606 *Quat Res*, 57, <https://doi.org/10.1006/qres.2001.2295>, 2002.
- 607 Spielhagen, R. F., Erlenkeuser, H., and Siebert, C.: History of freshwater runoff across the Laptev Sea
608 (Arctic) during the last deglaciation, *Glob Planet Change*, 48, 187–207,
609 <https://doi.org/10.1016/j.gloplacha.2004.12.013>, 2005.
- 610 Stuiver, M., Pearson, G. W., and Braziunas, T.: Radiocarbon Age Calibration of Marine Samples Back to
611 9000 Cal Yr BP, *Radiocarbon*, 28, <https://doi.org/10.1017/s0033822200060264>, 1986.
- 612 Svensson, A., Dahl-Jensen, D., Steffensen, J. P., Blunier, T., Rasmussen, S. O., Vinther, B. M.,
613 Vallelonga, P., Capron, E., Gkinis, V., Cook, E., Astrid Kjær, H., Muscheler, R., Kipfstuhl, S.,
614 Wilhelms, F., Stocker, T. F., Fischer, H., Adolphi, F., Erhardt, T., Sigl, M., Landais, A., Parrenin, F.,
615 Buizert, C., McConnell, J. R., Severi, M., Mulvaney, R., and Bigler, M.: Bipolar volcanic
616 synchronization of abrupt climate change in Greenland and Antarctic ice cores during the last glacial
617 period, *Climate of the Past*, 16, <https://doi.org/10.5194/cp-16-1565-2020>, 2020.
- 618 Wittmann, H., von Blanckenburg, F., Mohtadi, M., Christl, M., and Bernhardt, A.: The competition
619 between coastal trace metal fluxes and oceanic mixing from the $^{10}\text{Be}/^9\text{Be}$ ratio: Implications for
620 sedimentary records, *Geophys Res Lett*, 44, <https://doi.org/10.1002/2017GL074259>, 2017.



- 621 Wollenburg, J. E., Matthiessen, J., Vogt, C., Nehrke, G., Grotheer, H., Wilhelms-Dick, D., Geibert, W.,
622 and Mollenhauer, G.: Omnipresent authigenic calcite distorts Arctic radiocarbon chronology,
623 *Commun Earth Environ*, 4, <https://doi.org/10.1038/s43247-023-00802-9>, 2023.
- 624 Yiou, F., Raisbeck, G. M., Baumgartner, S., Beer, J., Hammer, C., Johnsen, S., Jouzel, J., Kubik, P. W.,
625 Lestringuez, J., Stiévenard, M., Suter, M., and Yiou, P.: Beryllium 10 in the Greenland Ice Core
626 Project ice core at Summit, Greenland, *J Geophys Res Oceans*, 102,
627 <https://doi.org/10.1029/97JC01265>, 1997.
- 628 Zheng, M., Liu, H., Adolphi, F., Muscheler, R., Lu, Z., Wu, M., and Prisle, N. L.: Simulations of 7 Be
629 and 10 Be with the GEOS-Chem global model v14.0.2 using state-of-the-art production rates,
630 *Geoscientific Model Development Discussions*, <https://doi.org/10.5194/gmd-2023-111>, 2023.
- 631
632